A Simple Route to Aqueous Suspensions of Degradable Copolymer Nanoparticles Based on Radical Ring-Opening Polymerization-Induced Self-Assembly (rROPISA)

Chen Zhu, Stéphanie Denis, Julien Nicolas

A Simple Route to Aqueous Suspensions of Degradable Copolymer Nanoparticles Based on Radical Ring-Opening Polymerization-Induced Self-Assembly (rROPISA)

Chen Zhu, Stéphanie Denis, Julien Nicolas[*]

Université Paris-Saclay, CNRS, Institut Galien Paris-Saclay, 92296

Châtenay-Malabry, France

*To whom correspondence should be addressed.

Email: julien.nicolas@u-psud.fr

Tel.: +33 1 46 83 58 53

Abstract

Degradable polymer nanoparticles are almost exclusively obtained by formulation of preformed degradable polymers, such as aliphatic polyesters, thus resulting is very low nanoparticle concentrations and limited structural diversity. On the other hand, many different vinyl polymers can be obtained by polymerization in aqueous dispersed media, but their non-degradability limits their use especially in the biomedical field. Herein, we combined the best of both worlds by developing a two-step radical ring-opening copolymerization-induced self-assembly (rROPISA) process, allowing to generate aqueous suspensions of narrowly dispersed, degradable vinyl copolymer nanoparticles at 15 wt.% solid contents, containing cyclic ketene acetal (CKA) units in the nanoparticle core. This strategy relied on rROPISA in DMF, followed by a simple transfer step to water. It was successfully applied to the three main CKAs used in rROP and yielded nanoparticles of ~80–215 nm in diameter with tunable amount of CKA up to 21 mol.%. Successful incorporation of ester groups in the copolymers was demonstrated by hydrolytic degradation of both the copolymers and the nanoparticles. The nanoparticles' cytocompatibility was then established by cell viability assays and cell morphology observation with three representative healthy cell lines. Not only this synthetic strategy could be of great potential for drug delivery applications, but it can also be beneficial to other research fields to yield more environmentally friendly materials involving the use of latexes, such as paints or coatings.

1. Introduction

Formulation of aqueous suspensions of degradable polymer nanoparticles has gained tremendous interest notably in the biomedical field.[1–4] Nanoparticles based on aliphatic polyesters are still considered to be the gold standard given their biodegradability and their FDA-approval for use in humans. However, polyester nanoparticles are exclusively obtained by formulation of preformed polymers using organic solvents because of the impossibility to perform their synthesis in water-borne conditions. It therefore results in very low concentrations in nanoparticles (ca 1–5 wt.%), which limits their use.[3] Moreover, compared to vinyl polymers, polyesters still suffer from limitations in terms of structural variation, functionalization and regarding the possibility to easily produce sophisticated architectures.

Conversely, vinyl polymers synthesized by reversible deactivation radical polymerization (RDRP) exhibit hight structural diversity, ease of functionalization and can be obtained in aqueous dispersed media to produce polymer (nano)particles. However, their non-degradability restricts their use for most biomedical applications because their lack of metabolization and/or excretion[4] can potentially lead to toxic accumulation of foreign materials in the body. Despite recent developments in radical ring-opening copolymerization (rROP) of cyclic ketene acetals (CKAs),[5–8] which is the most efficient strategy to insert ester groups in the backbone of vinyl polymers,

the preparation of aqueous suspensions of degradable nanoparticles by rROP is still at its infancy.[9] Therefore, a robust yet simple polymerization process able to produce aqueous suspensions of degradable polyester-like particles is still an unmet need. Such materials would indeed represent an important addition to the somewhat limited arsenal of degradable polymer nanoparticles available for biomedical applications and open new perspectives regarding environmentally friendly materials.

Among the different polymerization processes in dispersed media, polymerization-induced self-assembly (PISA)[10–12] has established as the most versatile and robust to generate a wide range of different diblock copolymer nano-object suspensions (e.g., spheres,[13] vesicles[14–16] or worms[17]) without surfactant and with high solids contents (ca 10–50 wt.%). PISA has indeed shown extraordinary flexibility in terms of polymerization techniques and conditions used,[18–20] monomers polymerized,[17,21–24] stimuli-responsiveness[23,25–28] or potential applications. However, even though PISA-derived nano-objects have been suggested for drug delivery or other biomedical applications,[13,21,29–35] there is yet no strategy to achieve aqueous suspension of degradable, polyester-like nanoparticles by PISA. Conversely, PISA was recently successfully applied to the synthesis of synthetic polypeptide nanoparticles by NCA polymerization.[36]

Herein, we tackled these challenges by developing a simple, yet robust two-step approach to generate aqueous suspensions of degradable polyester-like nanoparticles by PISA. To do so, we built on our recently developed rROPISA process,[37,38] a combination between PISA and rROP that served to produce nanoparticles in

non-polar solvents. In the present work, the rROPISA process was redesigned to make it fully compatible with the preparation of aqueous suspensions of degradable diblock copolymer nanoparticles (Figure 1). To demonstrate the flexibility of this process, it was successfully applied to the three main CKAs used in rROP; namely 2-methylene-4-phenyl-1,3-dioxolane (MPDL), 5,6-benzo-2-methylene-1,3-dioxepane (BMDO) and 2-methylene-1,3-dioxepane (MDO). Also, by a careful selection of the different polymer blocks, not only the nanoparticles exhibited a biocompatible shell,[39–43] but they also showed excellent cytocompatibility on representative healthy human cells.

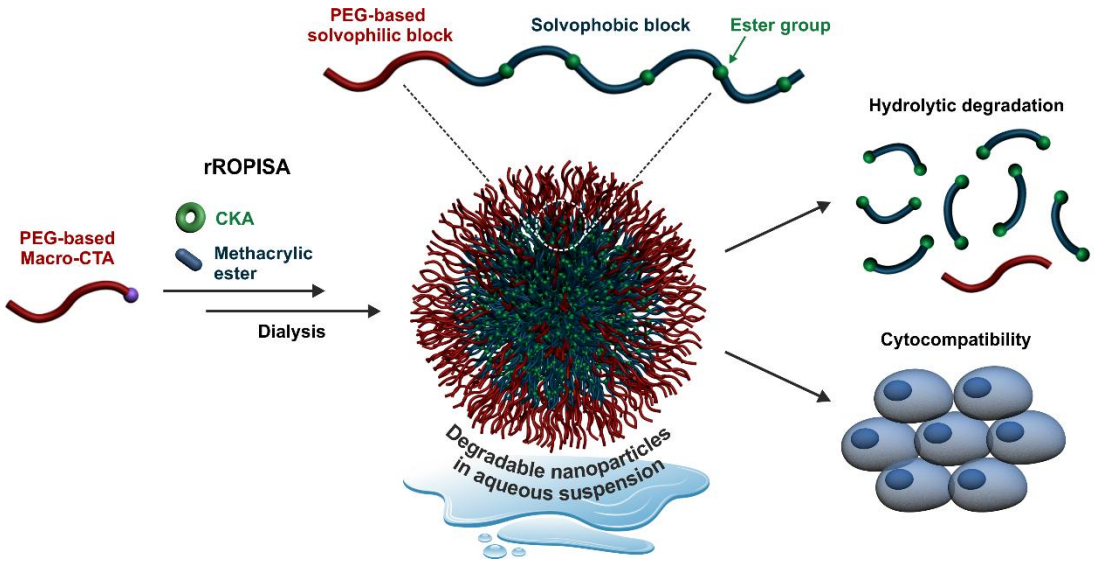

Figure 1. Synthesis of aqueous suspensions of core-degradable diblock copolymer nanoparticles by consecutive radical ring-opening copolymerization-induced self-assembly (rROPISA) from cyclic ketene acetals (CKAs), followed by transfer to water.

2. Materials and Methods

2.1. Materials

Lauryl methacrylate (LMA, 96%) and oligo(ethylene glycol) methyl ether methacrylate (OEGMA, M_n = 300 g.mol^{-1}) were purchased from Sigma-Aldrich and passed through basic alumina before use. 4-Cyano-4-[(dodecylsulfanylthiocarbonyl)sulfanyl]pentanoic acid (CDSPA, 97%), anhydrous *N*-*N*'-dimethylformamide (DMF) and 2,2′-azobis(2-methylpropionitrile) (AIBN, 98%) were purchased from Sigma-Aldrich and used as received. *Tert*-butyl peroxy-2-ethylhexanoate (Trigonox 21S or T21s) initiator was supplied by AkzoNobel. Deuterated chloroform ($CDCl_3$) and tetrahydrofuran (TDF) were obtained from Eurisotop. 2-Methylene-4-phenyl-1,3-dioxolane (MPDL), 2-methylene-1,3-dioxepane (MDO) and 5,6-benzo-2-methylene-1,3-dioxepane (BMDO) were prepared from the cyclic bromoacetal intermediate as described elsewhere.[44] All other solvents were purchased from Carlo-Erba and used as received. [3-(4,5-Dimethylthiazol-2-yl)-2,5-diphenyl tetrazolium bromide] (MTT) was purchased from Sigma-Aldrich and used as received.

2.2. Analytical method

2.2.1. Nuclear magnetic resonance (NMR) spectroscopy. ^{1}H-NMR spectroscopy was performed in 5 mm diameter tubes in deuterated chloroform ($CDCl_3$) or tetrahydrofuran (TDF) at 25 °C on a Bruker Avance 300 spectrometer at 300 MHz. The chemical shift scale was calibrated based on the internal solvent signal ($CDCl_3$: δ = 7.26 ppm; TDF: δ = 1.72 and 3.58 ppm).

2.2.2. Size exclusion chromatography (SEC). SEC was performed at 35 °C with two columns from Polymer Laboratories (PL-gel MIXED-D; 300 × 7.5 mm; bead diameter, 5 μm; linear part, 400−400 000 g.mol^{-1}) and a differential refractive index detector (Spectrasystem RI-150 from Thermo Electron Corp.). Chloroform was used as eluent at a flow rate of 1 mL.min^{-1} and toluene as a flow-rate marker. A conventional calibration curve was based on poly(methyl methacrylate) (PMMA) standards (peak molar masses, M_p = 625−625 500 g.mol^{-1}) from Polymer Laboratories. This technique allowed M_n (number-average molar mass), M_w (weight-average molar mass), and M_w/M_n (dispersity, $Đ$) to be determined. SEC of degraded copolymers was performed in the presence of 0.1 vol.% of trifluoroacetic acid (TFA, 99%) in chloroform (in both the mobile phase and the sample) to avoid the formation of aggregates and/or interaction with the columns because of carboxylic acid chain ends.

2.2.3. Dynamic light scattering (DLS). Nanoparticle diameters, reported in number (D_n), volume (D_v) and intensity (D_z), and particle size distribution (PSD) were measured by dynamic light scattering (DLS) with a Nano ZS from Malvern (173° scattering angle) at a temperature of 25 °C.

2.2.4. Transmission electron microscopy (TEM). Grids were glowing discharged before use. 5 µL of diluted nanoparticle suspensions (5 %, v/v) were deposited for 30 s on copper grids covered with formvar-carbon film. The excess solution was blotted off using a filter paper. Samples were then stained using uranyl acetate (2 %, w/v) for 1-5 min at room temperature. Then the excess solution was removed using a filter paper. The grids were then analyzed using a JEOL JEM-1400 operating at 80 kV. Images were acquired using an Orius camera (Gatan Inc, USA). The nanoparticles were analyzed by defining the number-average diameter (D_n), the weight-average diameter (D_w), the z-average diameter (D_z) and the polydispersity index (PDI) using the following equations:

$$D_n = \frac{\sum_i n_i \cdot D_i}{\sum_i n_i}$$

$$D_w = \frac{\sum_i n_i \cdot {D_i}^4}{\sum_i n_i \cdot {D_i}^3}$$

$$D_z = \frac{\sum_i n_i \cdot {D_i}^6}{\sum_i n_i \cdot {D_i}^5}$$

$PDI = D_w / D_n$

2.2.5. Cryogenic transmission electron microscopy (Cryo-TEM). Grids were prepared using a Vitrobot Mark IV (Thermo Fisher), operating at 20 °C and under 100 % humidity. 4 µL of undiluted nanoparticle suspensions were deposited on freshly glow discharged Quantifoil R2/2, 200 mesh grids. The grids were blotted for 5 s with blot force 0, and then plunge-frozen into liquid ethane cooled down at liquid nitrogen temperature. The grids were then analyzed using a Tecnai G20 (FEG, FEI) microscope operating at 200 kV, equipped with a K2 Summit direct-detection camera.

Images were recorded at 15.000 × magnification, with a pixel size of 2.5 Å at 20 $e^-/Å^2$.

2.2.6. Optical microscopy. Optical images of cells were captured with an AxioObserver Z1 (Carl Zeiss, Germany) inverted microscope equipped with a XL incubator thermostated at 37°C, a charge-coupled device (CCD) CoolSnap-HQ2 camera (6.45 µm pixel size; Photometrics, Tucson, USA) and an Achroplan 4X/0.10 NA dry objective lens using a brightfield mode (TL halogen lamp). Images (12 bits numerical) were processed using Zen 2.6 software (blue edition).

2.3. Synthetic procedures

2.3.1 Synthesis of poly[oligo(ethylene glycol) methyl ether methacrylate] (POEGMA) macro-chain transfer agent (CTA). The synthesis of $POEGMA_{23}$ was conducted as follows: in a 50 mL round bottom flask, fitted with a rubber septum and a magnetic stirring bar, a mixture of OEGMA (3.680 g, 0.012 mol), AIBN (9.6 mg, 5.93×10^{-2} mmol), CDSPA (0.097 g, 2.41×10^{-1} mmol, CDSPA/AIBN molar ratio = 4.0) and acetonitrile (25 mL) was degassed by argon bubbling for at least 15 min at room temperature. The mixture was then immersed in a preheated oil bath at 70 °C for 5 h. Monomer conversion was determined by ^1H NMR spectroscopy by integrating the two oxymethylene protons of OEGMA and POEGMA at 4.3 and 4.1 ppm, respectively. After the reaction, the polymer solution was cooled in an ice water bath. Acetonitrile was then removed under reduced pressure and the polymer was precipitated in a large excess of cold 1:1 diethyl ether/petroleum spirit mixture. The purified polymer was dried under high vacuum until constant weight. $DP_{n,NMR}$ was

determined by ^{1}H NMR spectroscopy by integrating the two oxymethylene protons of POEGMA at 4.1 ppm and the eighteen protons of the C_{12} alkyl chains of CDSPA at 1.2-1.4 ppm. $DP_{n,SEC}$, M_n and $Đ$ were obtained by SEC.

The same procedure was followed with the following modifications to obtain the $POEGMA_{52}$ macro-CTA: OEGMA (5.40 g, 0.018 mol), AIBN (4.5 mg, 2.78×10^{-2} mmol), CDSPA (0.050 g, 1.24×10^{-1} mmol) and acetonitrile (12.5 mL).

2.3.2. Block copolymer synthesis. For the sake of clarity, the following abbreviations will now be used: OEGMA = OEG, LMA = L, m = $DP_{n,POEGMA}$, n = $DP_{n,PLMA}$, POEGMA-*b*-PLMA = **OEG_m-L_n** (**MP0** and **MP5**), POEGMA-*b*-P(LMA-*co*-MPDL) = **OEG_m-L_nMP** (**MP1**-**MP9**), POEGMA-*b*-P(LMA-*co*-BMDO) = **OEG_m-L_nB** (**BM1**-**BM4**) and POEGMA-*b*-P(LMA-*co*-MDO) = **OEG_m-L_nM** (**M1**-**M4)**.

Synthesis of poly[oligo(ethylene glycol) methyl ether methacrylate]-b-poly[(lauryl methacrylate)-co-(2-methylene-4-phenyl-1,3-dioxolane)] (POEGMA-b-P(LMA-co-MPDL)). A typical synthesis of $POEGMA_{23}$-*b*-P(LMA_{150}-*co*-MPDL) (**OEG_{23}-L_{150}MP**) by RAFT dispersion polymerization at 15 wt.% solids with $f_{MPDL,0}$ = 0 (**MP0**) was as follows: in a 40 mL vial, fitted with a rubber septum and a magnetic stirring bar, a mixture of LMA (0.512 g, 2.02×10^{-3} mol), T21s initiator (0.6 mg, 2.78×10^{-3} mmol, dissolved at 0.1% w/v in DMF) and $POEGMA_{23}$ macro-CTA (0.098 g, 1.32×10^{-2} mmol; macro-CTA/initiator molar ratio = 5.0) in anhydrous DMF (3.41 g, 3.6 mL) was degassed by argon bubbling for at least 15 min and then immersed in a preheated oil bath at 90 °C for 24

h. Samples were periodically withdrawn to determine the LMA conversion by ^{1}H NMR spectroscopy by integrating the two oxymethylene protons of LMA at 5.5 and 6.0 ppm with PLMA protons at 3.8 ppm. M_n and $Đ$ were determined by SEC. The nanoparticle colloidal characteristics, D_z and PSD, were obtained by DLS. The nanoparticles were dried under reduced pressure at 40 °C and solubilized in a minimal amount of dichloromethane (DCM) before precipitation in cold methanol. The purified copolymer was collected after centrifugation (10 000 rpm, 30 min) and dried under high vacuum until constant weight.

The same procedure was performed with: $f_{MPDL,0}$ = 0.2 (**MP1**) [LMA (0.504 g, 1.99 × 10^{-3} mol), MPDL (0.081 g, 5.00 × 10^{-1} mmol), T21s initiator (0.6 mg, 2.78 × 10^{-3} mmol, dissolved at 0.1% w/v in DMF), $POEGMA_{23}$ macro-CTA (0.102 g, 1.38 × 10^{-2} mmol, DMF (3.9 g, 4.1 mL)]; $f_{MPDL,0}$ = 0.4 (**MP2**) [LMA (0.511 g, 2.01 × 10^{-3} mol), MPDL (0.214 g, 1.32 × 10^{-3} mol), T21s initiator (0.6 mg, 2.78 × 10^{-3} mmol, dissolved at 0.1% w/v in DMF), $POEGMA_{23}$ macro-CTA (0.103 g, 1.39 × 10^{-2} mmol) and DMF (4.7 g, 5.0 mL)]; $f_{MPDL,0}$ = 0.6 (**MP3**) [LMA (0.507 g, 2.00 × 10^{-3} mol), MPDL (0.476 g, 2.94 × 10^{-3} mol), T21s initiator (0.6 mg, 2.78 × 10^{-3} mmol, dissolved at 0.1% w/v in DMF), $POEGMA_{23}$ macro-CTA (0.095 g, 1.28 × 10^{-2} mmol) and DMF (6.2 g, 6.5 mL)] and $f_{MPDL,0}$ = 0.7 (**MP4**) [LMA (0.500 g, 1.97 × 10^{-3} mol), MPDL (0.785 g, 4.85 × 10^{-3} mol), T21s initiator (0.6 mg, 2.78 × 10^{-3} mmol, dissolved at 0.1% w/v in DMF) and $POEGMA_{23}$ macro-CTA (0.099 g, 1.34 × 10^{-2} mmol) and DMF (7.6 g, 8.0 mL)].

The same procedure was performed with $POEGMA_{52}$ macro-CTA, a targeted $DP_{n,PLMA}$ = 300 (**OEG_{52}-L_{300}MP**) and with: $f_{MPDL,0}$ = 0 (**MP5**) [LMA (0.503 g, 1.98 × 10^{-3} mol), T21s initiator (0.2 mg, 9.26 × 10^{-4} mmol, dissolved at 0.1% w/v in DMF) and $POEGMA_{52}$ macro-CTA (0.107 g, 6.65 × 10^{-3} mmol) and DMF (3.5 g, 3.7 mL)]; $f_{MPDL,0}$ = 0.2 (**MP6**) [LMA (0.500 g, 1.97 × 10^{-3} mol), MPDL (0.082 g, 5.06 × 10^{-1} mmol), T21s initiator (0.3 mg, 1.39 × 10^{-3} mmol, dissolved at 0.1% w/v in DMF) and $POEGMA_{52}$ macro-CTA (0.105 g, 6.52 × 10^{-3} mmol) and DMF (3.9 g, 4.1 mL)]; $f_{MPDL,0}$ = 0.4 (**MP7**) [LMA (0.503 g, 1.98 × 10^{-3} mol), MPDL (0.215 g, 1.33 × 10^{-3} mol), T21s initiator (0.2 mg, 9.26 × 10^{-4} mmol, dissolved at 0.1% w/v in DMF) and $POEGMA_{52}$ macro-CTA (0.107 g, 6.65 × 10^{-3} mmol) and DMF (4.6 g, 4.9 mL)]; $f_{MPDL,0}$ = 0.6 (**MP8**) [LMA (0.510 g, 2.01 × 10^{-3} mol), MPDL (0.476 g, 2.94 × 10^{-3} mol), T21s initiator (0.2 mg, 9.26 × 10^{-4} mmol, dissolved at 0.1% w/v in DMF) and $POEGMA_{52}$ macro-CTA (0.107 g, 6.65 × 10^{-3} mmol) and DMF (6.1 g, 6.4 mL)] and $f_{MPDL,0}$ = 0.7 (**MP9**) [LMA (0.501 g, 1.97 × 10^{-3} mol), MPDL (0.758 g, 4.68 × 10^{-3} mol), T21s initiator (0.2 mg, 9.26 × 10^{-4} mmol, dissolved at 0.1% w/v in DMF) and $POEGMA_{52}$ macro-CTA (0.107 g, 6.65 × 10^{-3} mmol) and DMF (7.6 g, 8.0 mL)].

Synthesis of poly[oligo(ethylene glycol) methyl ether methacrylate]-b-poly[(lauryl methacrylate)-co-(5,6-benzo-2-methylene-1,3-dioxepane)] (POEGMA-b-P(LMA-co-BMDO)). A typical synthesis of $POEGMA_{23}$-*b*-P(LMA_{150}-*co*-BMDO) (**OEG_{23}-L_{150}B**) by RAFT dispersion polymerization at 15 wt.% solids and $f_{BMDO,0}$ = 0.2 (**BM1**) was as follows: in a 40 mL

vial, fitted with a rubber septum and a magnetic stirring bar, a mixture of LMA (0.514 g, 2.02 × 10^{-3} mol), BMDO (0.080 g, 4.91 × 10^{-1} mmol), T21s initiator (0.6 mg, 2.78 × 10^{-3} mmol, dissolved at 0.1% w/v in DMF) and $POEGMA_{23}$ macro-CTA (0.101 g, 1.37 × 10^{-2} mmol; macro-CTA/initiator molar ratio = 5.0) in anhydrous DMF (3.8 g, 4.0 mL) was degassed by argon bubbling for at least 15 min and then immersed in a preheated oil bath at 90 °C for 24 h. Determination of LMA conversion and colloidal characteristics of the nanoparticles as well as purification of the copolymers were performed as for **OEG_{23}-L_{150}MP.**

The same procedure was performed with: $f_{BMDO,0}$ = 0.4 (**BM2**) [LMA (0.501 g, 1.97 × 10^{-3} mol), BMDO (0.241 g, 1.48 × 10^{-3} mol), T21s initiator (0.6 mg, 2.78 × 10^{-3} mmol, dissolved at 0.1% w/v in DMF) and $POEGMA_{23}$ macro-CTA (0.096 g, 1.30 × 10^{-2} mmol) and DMF (4.6 g, 4.9 mL)]; $f_{BMDO,0}$ = 0.6 (**BM3**) [LMA (0.503 g, 1.98 × 10^{-3} mol), BMDO (0.482 g, 2.96 × 10^{-3} mol), T21s initiator (0.6 mg, 4.17 × 10^{-3} mmol, dissolved at 0.1% w/v in DMF) and $POEGMA_{23}$ macro-CTA (0.099 g, 1.34 × 10^{-2} mmol) and DMF (6.1 g, 6.4 mL)]; $f_{BMDO,0}$ = 0.7 (**BM4**) [LMA (0.504 g, 1.98 × 10^{-3} mol), BMDO (0.805 g, 4.94 × 10^{-3} mol), T21s initiator (0.6 mg, 2.78 × 10^{-3} mmol, dissolved at 0.1% w/v in DMF) and $POEGMA_{23}$ macro-CTA (0.098 g, 1.32× 10^{-2} mmol) and DMF (7.6 g, 8.0 mL)].

Synthesis of poly[oligo(ethylene glycol) methyl ether methacrylate]-b-poly[(lauryl methacrylate)-co-(2-methylene-1,3-dioxepane)] (POEGMA-b-P(LMA-co-MDO)). A typical synthesis of $POEGMA_{23}$-*b*-$P(LMA_{150}$-*co*-MDO) (**OEG_{23}-L_{150}M**) by RAFT dispersion

polymerization at 15 wt.% solids with $f_{MDO,0}$ = 0.2 (**M1)** was as follows: in a 40 mL vial, fitted with a rubber septum and a magnetic stirring bar, a mixture of LMA (0.532 g, 2.09 × 10^{-3} mol), MDO (0.059 g, 5.18 × 10^{-1} mol), T21s initiator (0.6 mg, 2.78 × 10^{-3} mmol, dissolved at 0.1% w/v in DMF) and $POEGMA_{23}$ macro-CTA (0.095g, 1.28 × 10^{-2} mmol; macro-CTA/initiator molar ratio = 5.0) in anhydrous DMF (3.7 g, 3.9 mL) was degassed by argon bubbling for at least 15 min and then immersed in a preheated oil bath at 90 °C for 24 h. Determination of LMA conversion and colloidal characteristics of the nanoparticles as well as purification of the copolymers were performed as for **OEG_{23}-L_{150}MP.**

The same procedure was performed with $f_{MDO,0}$ = 0.4 (**M2**) [LMA (0.520 g, 2.05 × 10^{-3} mol), MDO (0.150 g, 1.32 × 10^{-3} mol), T21s initiator (0.6 mg, 2.78 × 10^{-3} mmol, dissolved at 0.1% w/v in DMF) and $POEGMA_{23}$ macro-CTA (0.098 g, 1.32 × 10^{-2} mmol) and DMF (4.3 g, 4.5 mL)], $f_{MDO,0}$ = 0.6 (**M3**) [LMA (0.510 g, 2.01 × 10^{-3} mol), MDO (0.340 g, 2.98 × 10^{-3} mol), T21s initiator (0.6 mg, 2.78 × 10^{-3} mmol, dissolved at 0.1% w/v in DMF) and $POEGMA_{23}$ macro-CTA (0.095 g, 1.28 × 10^{-2} mmol) and DMF (5.5 g, 5.8 mL)] and $f_{MDO,0}$ = 0.7 (**M4**) [LMA (0.504 g, 1.98 × 10^{-3} mol), MDO (0.524 g, 4.60 × 10^{-3} mol), T21s initiator (0.6 mg, 4.17 × 10^{-3} mmol, dissolved at 0.1% w/v in DMF) and $POEGMA_{23}$ macro-CTA (0.099 g, 1.34 × 10^{-2} mmol) and DMF (6.4 g, 6.8 mL)].

2.4. Degradation procedures

2.4.1. Polymer degradation. In a 5 mL vial, 50 mg of purified copolymer was dissolved in 2.5 mL of THF. After solubilization, 2.5 mL of potassium hydroxide

solution (KOH, 5 wt.%) in MeOH was added. The cloudy mixture was stirred at room temperature. Samples (1 mL) were periodically withdrawn, immediately dried under vacuum and mixed with 2 mL of chloroform, allowing salts filtration using a 0.2 μm PTFE filter. After filtration, the organic phase was washed three times with HCl (1 mL, 1 mol.L^{-1}). The organic solvent was then removed under reduced pressure and the degradation products were analyzed by SEC with 0.1 vol.% TFA in the eluent.

2.4.2. Nanoparticle degradation. In a 40 mL vial were mixed an aqueous suspension of nanoparticles and an equal volume of aqueous potassium hydroxide (KOH, 5 wt.%). The vial was placed in an orbital shaker (IKA KS4000i control, 37°C, 90 rpm) and samples were withdrawn at different intervals and lyophilized. 2 mL of chloroform was then added to each vial allowing salts filtration by using a 0.2 μm PTFE filter. After filtration, the organic phase was washed three times with HCl (1 mL, 1 mol.L^{-1}). The organic solvent was then removed under reduced pressure and the degradation products were analyzed by SEC with 0.1 vol.% TFA in the eluent.

2.5. Transfer procedures to water

2.5.1. Dialysis against water. A suspension of nanoparticles was directly poured into a pre-wetted dialysis bag (MWCO 3500, RC membrane) and then dialyzed against water. Water was changed twice a day for three days. The same procedure was also performed except the nanoparticle suspension was diluted 20 times in DMF before dialysis.

2.5.2. Dialysis with an intermediate solvent. A suspension of nanoparticles was directly poured into a pre-wetted dialysis bag (MWCO 3500, RC membrane) and then

dialyzed against acetone. Acetone was changed twice a day for three days. After dialysis, the acetone suspension of nanoparticles was transferred to another dialysis bag (MWCO = 3500, RC membrane) and dialyzed against water. Water was changed twice a day for three days.

2.5.3. Nanoprecipitation procedure. In a 7-mL vial, the purified copolymer (10 mg) was solubilized in 0.1 mL of THF and this solution was added dropwise to different volumes of MiliQ water (0.5, 1, 2 or 5 mL) to reach the desired concentrations of nanoparticles under stirring (700 rpm). THF was then gently removed under reduced pressure. The resulting nanoparticle suspension was analyzed by DLS.

2.6. Biological evaluation

2.6.1 Cell culture. Human endothelial umbilical vein cells (HUVEC), embryonic murine fibroblast (NIH/3T3) and murine macrophage-monocyte cells (J774.A1) were purchased from American Type Culture Collection (ATCC) and maintained as recommended. Fetal Bovine Serum (FBS) was purchased from Gibco, Penicillin-Streptomycin stabilized solution, Dulbecco's Modified Eagle Medium (DMEM) and Roswell Park Memorial Institute medium (RPMI)-1640 medium were purchased from Sigma-Aldrich and used as received. J774.A1 cells were grown in RPMI-1640 supplemented with 10 % FBS, penicillin (50 $U.mL^{-1}$) and streptomycin (50 $U.mL^{-1}$). NIH/3T3 and HUVEC cells were grown in DMEM high glucose supplemented with 10 % FBS, penicillin (50 $U.mL^{-1}$) and streptomycin (50 $U.mL^{-1}$). Cells were maintained in a humid atmosphere at 37 °C with 5 % CO_2.

2.6.2 Cell viability assay. In 96-well microtiter plates (TPP, Switzerland), cells were seeded (HUVEC: 2×10^4 cells mL^{-1}, NIH/3T3: 4×10^4 cells mL^{-1}, J774.A1: 2×10^4 cells mL^{-1}) in 100 µL of growth medium and preincubated for 24 h in incubator (37 °C and 5% CO_2). After appropriate dilutions, 100 µL of the copolymer nanoparticles (obtained after intermediate dialysis in acetone to remove remaining monomer, see part 3.3) in cell culture medium (0.01, 0.05, 0.1 and 0.5 $mg.mL^{-1}$) was added over the cells and incubated for 72 h. A MTT solution (5 $mg.mL^{-1}$) was prepared with phosphate buffered saline (PBS) and filtered with sterile filters (0.2 µm). At the end of incubation period, 20 µL of MTT solution was added to each well. After incubation (1 h for HUVEC and J774.A1 cells, 1.5 h for NIH/3T3 cells), the medium was removed and 200 µL of dimethylsulfoxide (DMSO) was then added to each well to dissolve the formazan crystals. The absorbance was then measured by a microplate reader (LAB Systems Original Multiscan MS) at 570 nm. Cell viability was calculated as the absorbance ratio between treated and untreated control cells. All experiments were performed in triplicate to determine means and SD.

3. Results and Discussion

3.1 Design rationale

Previous work in rROPISA was limited to the synthesis of non-aqueous suspensions of CKA-containing poly(lauryl methacrylate)-*b*-poly(benzyl methacrylate) (PLMA-*b*-PBzMA) nanoparticles in heptane to prevent early hydrolysis of CKA

monomers/repeat units.[38,45] Their hydrophobic PLMA stabilizing shell therefore prevents any subsequent transfer to aqueous media. In this context, we designed a simple two-step rROPISA system allowing for the synthesis of stable aqueous suspensions of degradable particles by first performing rROPISA in DMF as a water-miscible polar solvent, followed by transfer of the particles to water during which their colloidal properties were preserved.

The idea was to choose poly[oligo(ethylene glycol) methyl ether methacrylate] (POEGMA) as the solvophilic block given its solubility in both water and many polar organic solvents including DMF (Figure 2). Also, POEGMA is a well-known PEG-based polymer used in the biomedical field, owing to its biocompatibility and to the stealth properties it confers to nanoparticles or therapeutics.[39–43,46–48] PLMA was selected as a solvophobic block according to its non-solubility in DMF and the ability of LMA to copolymerize with CKAs such as MPDL and BMDO.[38] These two aromatic ring-containing CKAs were first tested before investigating the use of MDO, whose polymer has the same structure as polycaprolactone (without the presence of branching), a well-known polymer approved for use in humans.[49]

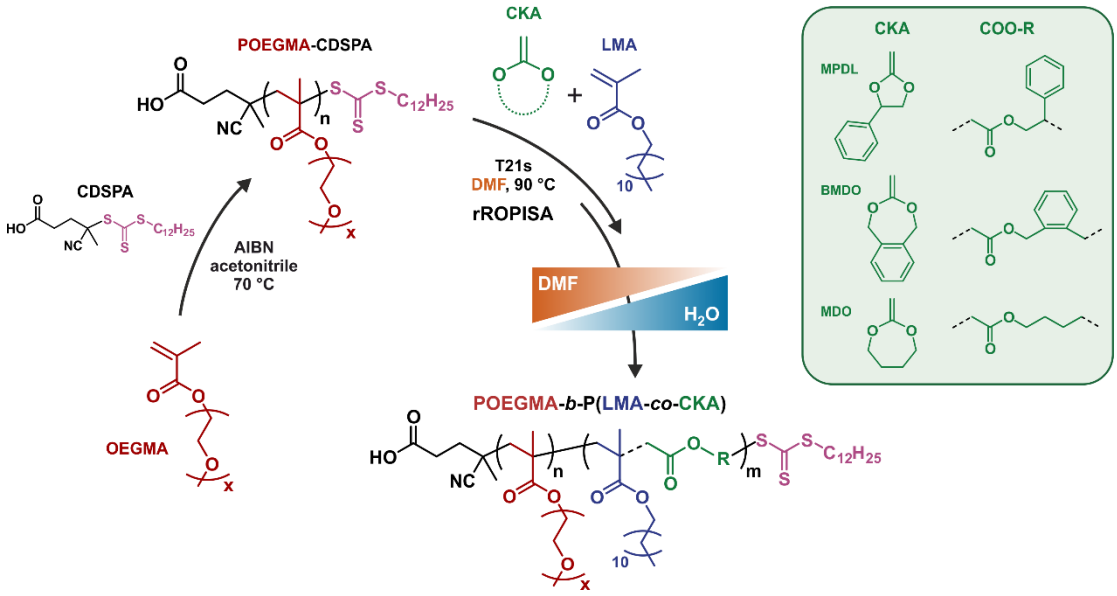

Figure 2. RAFT-mediated synthesis of poly[oligo(ethylene glycol) methyl ether methacrylate)] (POEGMA) chain transfer agent followed by radical ring-opening copolymerization-induced self-assembly (rROPISA) in DMF at 90°C of lauryl methacrylate (LMA) and cyclic ketene acetals (CKAs), followed by transfer to water to produce aqueous suspensions of POEGMA-*b*-P(LMA-*co*-CKA) (**OEG$_m$-L$_n$CKA**) diblock copolymer nanoparticles.

3.2 Application to the three main CKAs

3.2.1 Application to MPDL. Well-defined POEGMA$_{23}$ ($M_{n,SEC}$ = 7 400 g.mol^{-1}, $Đ$ = 1.09) and POEGMA$_{52}$ ($M_{n,SEC}$ = 16 100 g.mol^{-1}, $Đ$ = 1.15) macro-CTAs were first synthesized by RAFT solution polymerization of OEGMA in acetonitrile at 70 °C for 5 h using CDSPA as a CTA and AIBN as a radical initiator (Table S1, Figure S1).

The POEGMA$_{23}$ macro-CTA was then chain-extended by copolymerization of LMA (targeted $DP_{n,PLMA}$ = 150) with variable initial amounts of MPDL ($f_{MPDL,0}$ = 0–0.7) at 15 wt.% solids in DMF at 90 °C in the presence of T21s as a radical initiator (**OEG$_{23}$-L$_{150}$MP**, **MP0-MP4**, Figure 2). After 24 h, high monomer conversions (~80–90 %) were obtained except for **MP3** ($f_{MPDL,0}$ = 0.6) and **MP4** ($f_{MPDL,0}$ = 0.7),

for which the polymerization kinetics were slower (Table S2 and Figure 3a). Linear evolutions of M_n values with conversion and reasonably low dispersities ($Đ$ = 1.2–1.4 below 50% conversion) were obtained for all copolymerizations (Figure 3b), with no noticeable impact of the presence of MPDL when compared to **MP0** ($f_{MPDL,0}$ = 0).

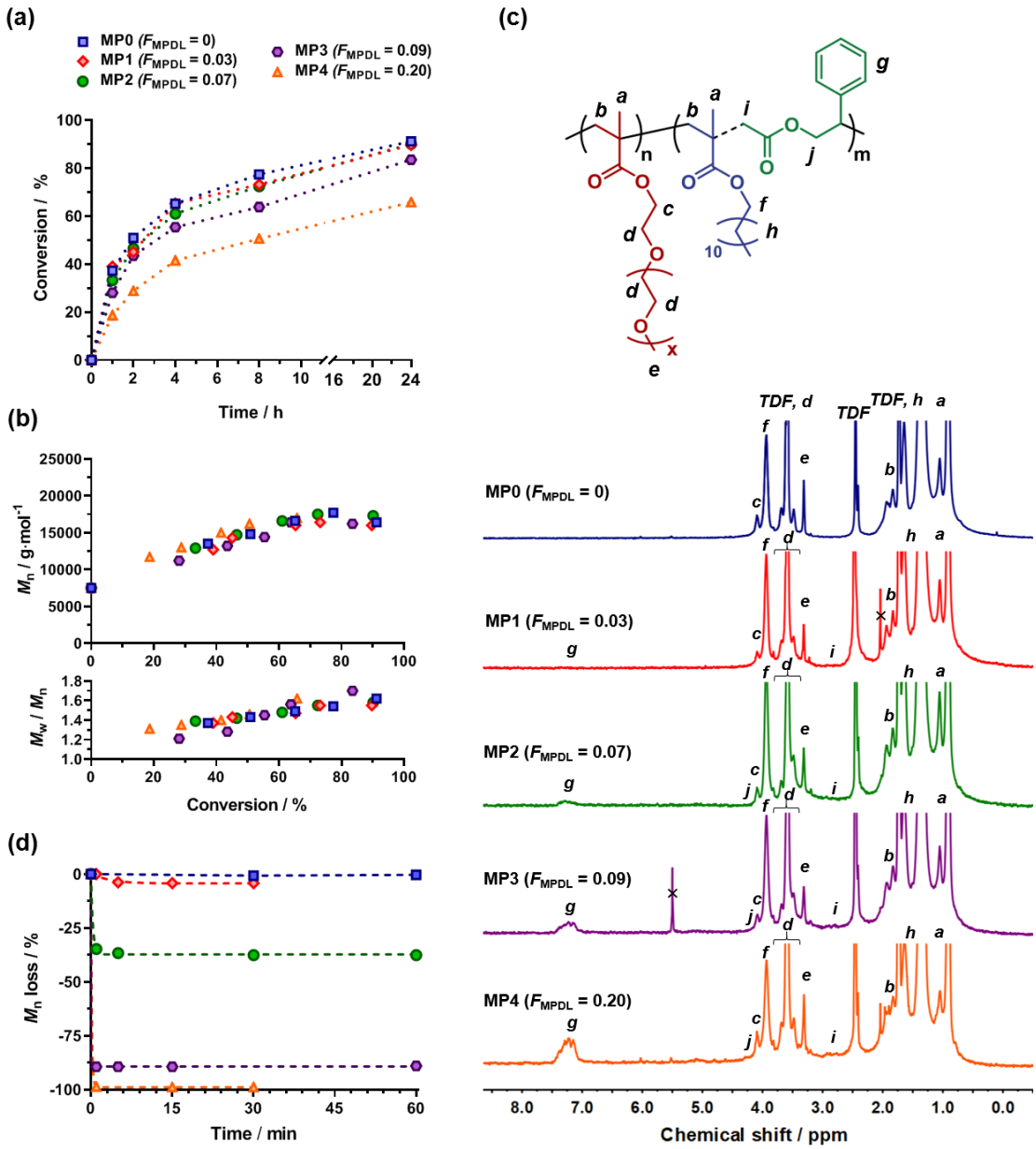

Figure 3. Synthesis of **OEG_{23}-L_{150}MP** copolymer nanoparticles (**MP0-MP4**) by RAFT-mediated dispersion copolymerization of LMA and MPDL from a $POEGMA_{23}$ macro-CTA in DMF at 90 °C as function of $f_{MPDL,0}$: (a) LMA conversion vs. time (dashed lines connecting data points are guides for the eye only); (b) M_n and dispersity (M_w/M_n) of the

copolymers vs. LMA conversion determined by SEC; (c) ^{1}H NMR spectra in TDF of the copolymers in the 0–8.5 ppm region (crosses indicate residual solvent) and (d) evolution with time of their M_n loss during degradation under accelerated conditions (dashed lines represent the exponential one phase decay fits). Since SEC is known to overestimate the molar masses at the low-molar-mass region, these values should be taken with care.

The structure of POEGMA-*b*-P(LMA-*co*-MPDL) copolymers was confirmed by ^{1}H NMR spectroscopy (Figure 3c), with in particular, the successful insertion of MPDL as shown by the aromatic protons *g*. Their integration increased with $f_{MPDL,0}$ and gave molar fractions in the copolymer, F_{MPDL}, ranging from 0 to 0.20 (Table S2). The observed discrepancies between $f_{MPDL,0}$ and F_{MPDL} values are explained by unfavorable reactivity ratios between CKAs and methacrylic esters, resulting in gradient-type copolymers. The presence of ester groups in the copolymer was confirmed by hydrolytic degradation under accelerated conditions (THF/MeOH, KOH 2.5 wt.%). While **MP0** ($f_{MPDL,0}$ = 0) let the M_n unchanged, **MP1-MP4** ($f_{MPDL,0}$ = 0.2–0.7) copolymers gave a decrease in M_n (Figure 3d), as shown by the relatively homogeneous shifts of the SEC chromatograms towards lower M_n values (Figure S2), suggesting a relatively weak gradient character. As expected, the higher F_{MPDL} (or $f_{MPDL,0}$), the lower the copolymerization rate and the lower the final M_n after degradation, that reached 25 000, 13 100, 2 700 and 200 g.mol^{-1} for F_{MPDL} = 0.03, 0.07, 0.09 and 0.20, respectively (Table S3). Those values are in the same order of magnitude than the theoretical ones for the highest amounts of MPDL (Table S3). The discrepancy at low MPDL contents may be can be explained by the non-negligible amount of closed MPDL units in the copolymer, as already seen with this CKA.[50]

The onset of the micellar nucleation and the formation of particles occurred after 0.5-1 h, as evidenced by the change in appearance of the polymerization medium from transparent to opalescent. After the polymerizations, stable suspensions of POEGMA-*b*-P(LMA-*co*-MPDL) nanoparticles in DMF were obtained exhibiting average intensity-diameters (D_z) in the 72–109 nm range and particle size distributions (PSD) all below 0.1, indicating narrowly dispersed nanoparticles (Table S2).

The **OEG_{23}-L_{150}MP** nanoparticles were then transferred to water through a simple dialysis step. Direct dialysis against water gave stable nanoparticle suspensions only for $F_{MPDL} \leq 0.07$, likely because of the strong hydrophobicity of unreacted MPDL that altered the colloidal stability. However, when all nanoparticles were diluted 1:20 with DMF prior dialysis, highly stable nanoparticles with narrow PSD (0.01–0.03) were obtained for all F_{MPDL} values (Table S2, Figure 4 and S3). Importantly, their average diameters were preserved after dialysis, with however a noticeable increase in the nanoparticles' size for high MPDL contents (Figure 4a–e). TEM experiments revealed the formation of nanoparticles with spherical morphology (Figure 4f–o). Their average diameters and size distributions were in good agreement with DLS data except for the copolymer with the highest amount of MPDL whose PSD was already broad according to DLS, presumably due to the presence of micro-particle aggregates during TEM sample preparation. All nanoparticles also exhibited very high colloidal stability with no or little variation of their average diameters or their dispersity (PSD = 0.01–0.03) after at least 9 months (Figure 4a–e),

which demonstrated the robustness of the 2-step rROPISA process for the preparation of stable aqueous suspensions of CKA-containing nanoparticles.

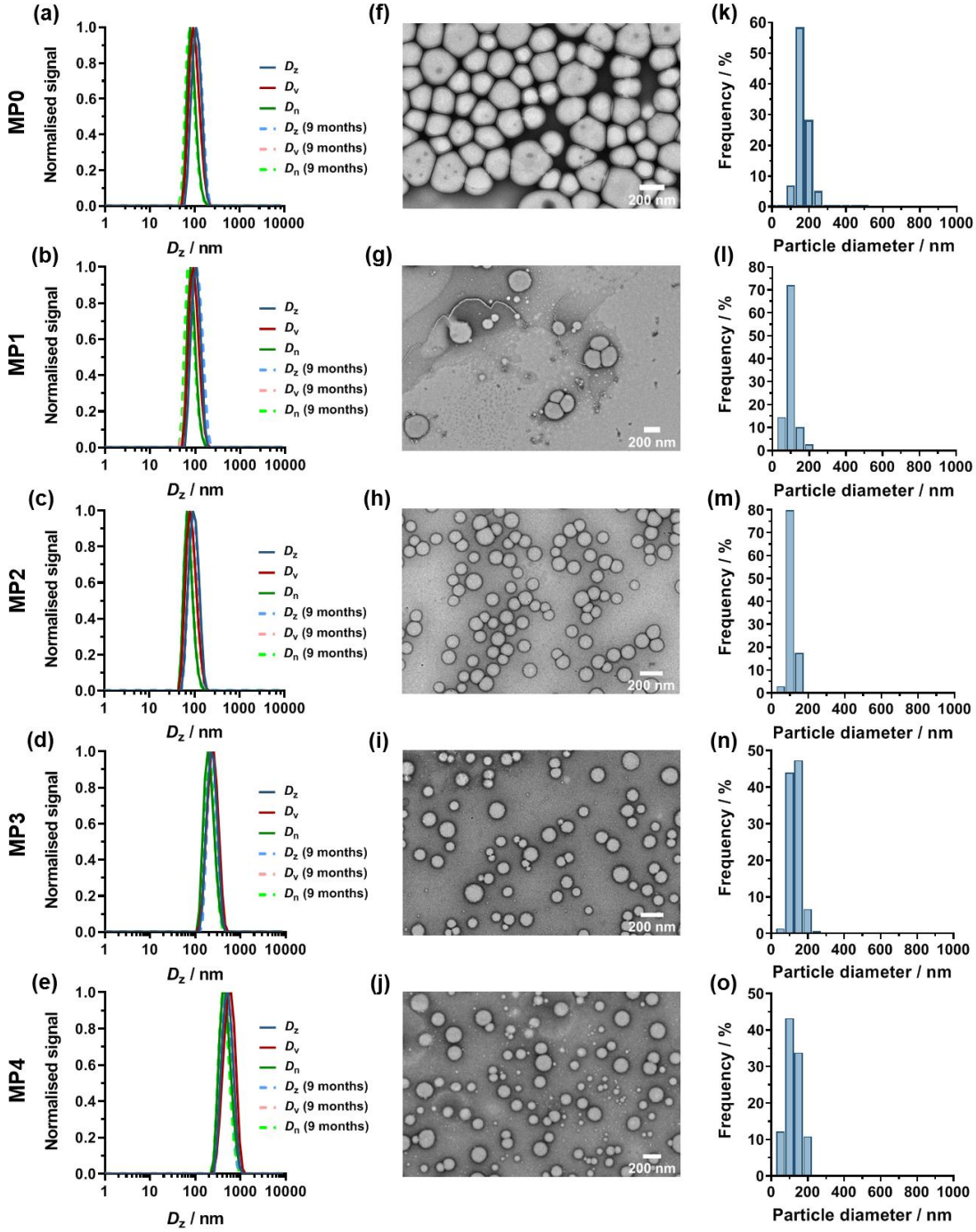

Figure 4. Colloidal characteristics of **OEG$_{23}$-L$_{150}$MP** nanoparticles **MP0–MP4** after a 1:20 dilution in DMF and dialysis against water: (a–e) average diameters from DLS reported in number (D_n), volume (D_v) and intensity (D_z) distribution after formulation and after 9 months;

(f–j) representative TEM images and (k–o) particle size distributions (n = 75–800). TEM data (D_n, D_w, D_z, and PDI) are in Table S4.

Similar rROPISA experiments were then performed with the longest macro-CTA ($POEGMA_{52}$) to potentially improve the preservation of the nanoparticles' colloidal properties at high MPDL contents upon their transfer to water, as suggested by its superior stabilization properties during rROPISA in heptane.[51] Copolymerizations of LMA (targeted $DP_{n,PLMA}$ = 300) and MPDL ($f_{MPDL,0}$ = 0–0.7) were performed in DMF under the same experimental conditions as previously described in order to produce **OEG_{52}-L_{300}MP** copolymer nanoparticles (**MP5**–**MP9**, Table S2). Very similar results in terms of conversions (70–88%) and control of the polymerizations (M_n = 37.0–22.9 kg.mol^{-1}, $Đ$ = 1.54–1.86) were obtained, with however an overall increase in size of the nanoparticles (D_z = 113–168 nm, PSD = 0.10–0.22). Interestingly, the MPDL contents were also mostly higher (Table S2, Figure S4a), resulting in more pronounced hydrolytic degradation under accelerated conditions for **OEG_{52}-L_{300}MP** copolymers than the **OEG_{23}-L_{150}MP** counterparts for the same $f_{MPDL,0}$ value (Figure S2 and S4b). It also resulted in a slightly better agreement between predicted and experimental M_n values after degradation (Table S5).

Dialysis of **OEG_{52}-L_{300}MP** nanoparticles against water also led to stable aqueous suspensions of spherical nanoparticles with narrow PSD as shown by DLS and TEM (Table S2 and S4, Figure S3 and S5). Interestingly, conversely to **OEG_{23}-L_{150}MP** nanoparticles, they exhibited a much better preservation of their colloidal characteristics even for nanoparticles with the highest MPDL contents (Table S2 and

Figure 5), together with a better agreement between average diameters determined by DLS and TEM.

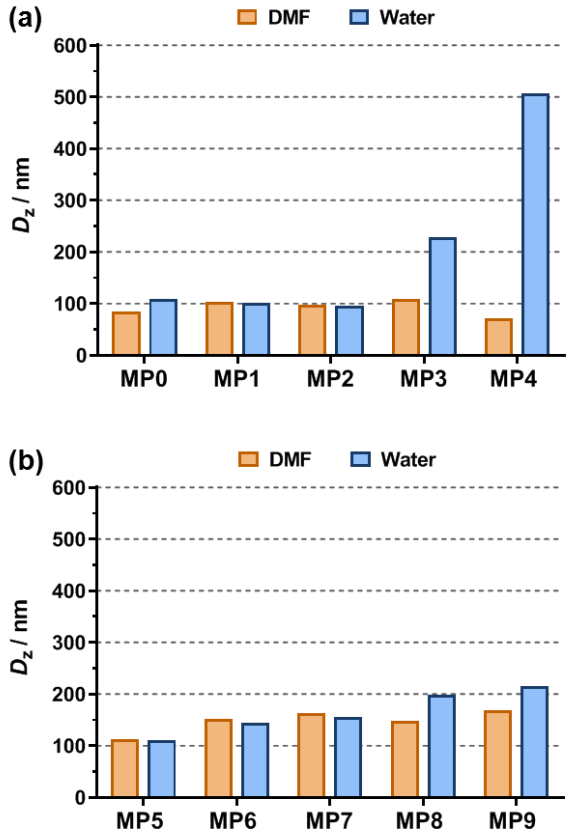

Figure 5. Intensity-average diameters (D_z) of: (a) **OEG$_{23}$-L$_{150}$MP** (**MP0-MP4**) and (b) **OEG$_{52}$-L$_{300}$MP** (**MP5-MP9**) nanoparticles in DMF (orange bars) and after a 1:20 dilution in DMF followed by dialysis against water (blue bars).

3.2.2 Application to BMDO. The 2-step rROPISA process was then successfully applied to BMDO, which is still one of the most popular CKAs used in rROP. **OEG$_{23}$-L$_{150}$B** copolymers nanoparticles were obtained by chain-extension of POEGMA$_{23}$ macro-CTA by copolymerization of LMA and BMDO ($f_{BMDO,0}$ = 0.2–0.7) under the same experimental conditions as for **OEG$_{23}$-L$_{150}$MP** copolymers (Figure S6 and Table S6). In general, very similar results were obtained compared to MPDL.

However, a better control of the polymerizations was achieved ($Đ$ = 1.23–1.50), together with a slight increase in the BMDO content in the obtained copolymers (Table S6).

Degradation of **OEG$_{23}$-L$_{150}$B** copolymers under accelerated conditions confirmed their tunable degradability as function of $f_{BMDO,0}$ (Table S7, Figure S6b and S7a–d). The degradation was very similar to that of **OEG$_{23}$-L$_{150}$MP** copolymers with nonetheless a much more pronounced decrease in M_n when $f_{BMDO,0}$ = 0.4 (-75% vs. -38%) owing to its higher BMDO content (F_{BMDO} = 0.15 vs. F_{MPDL} = 0.07).

Narrowly dispersed nanoparticles were also obtained (PSD $\leq$ 0.06), but with smaller diameters (D_z = 53–78 nm) than MPDL-containing nanoparticles (Table S6). After diluted dialysis against water, very stable nanoparticles were obtained and with average diameters in the range 93–161 nm and excellent retention of their narrow PSD (Figure 6 and S3). Interestingly, no significant size increase was obtained for **OEG$_{23}$-L$_{150}$B** nanoparticles with the highest amounts of BMDO, as they all remained below 200 nm in diameter (Figure S8a). The colloidal properties obtained by TEM were in good agreement with DLS measurements and also showed spherical morphologies (Figure 6).

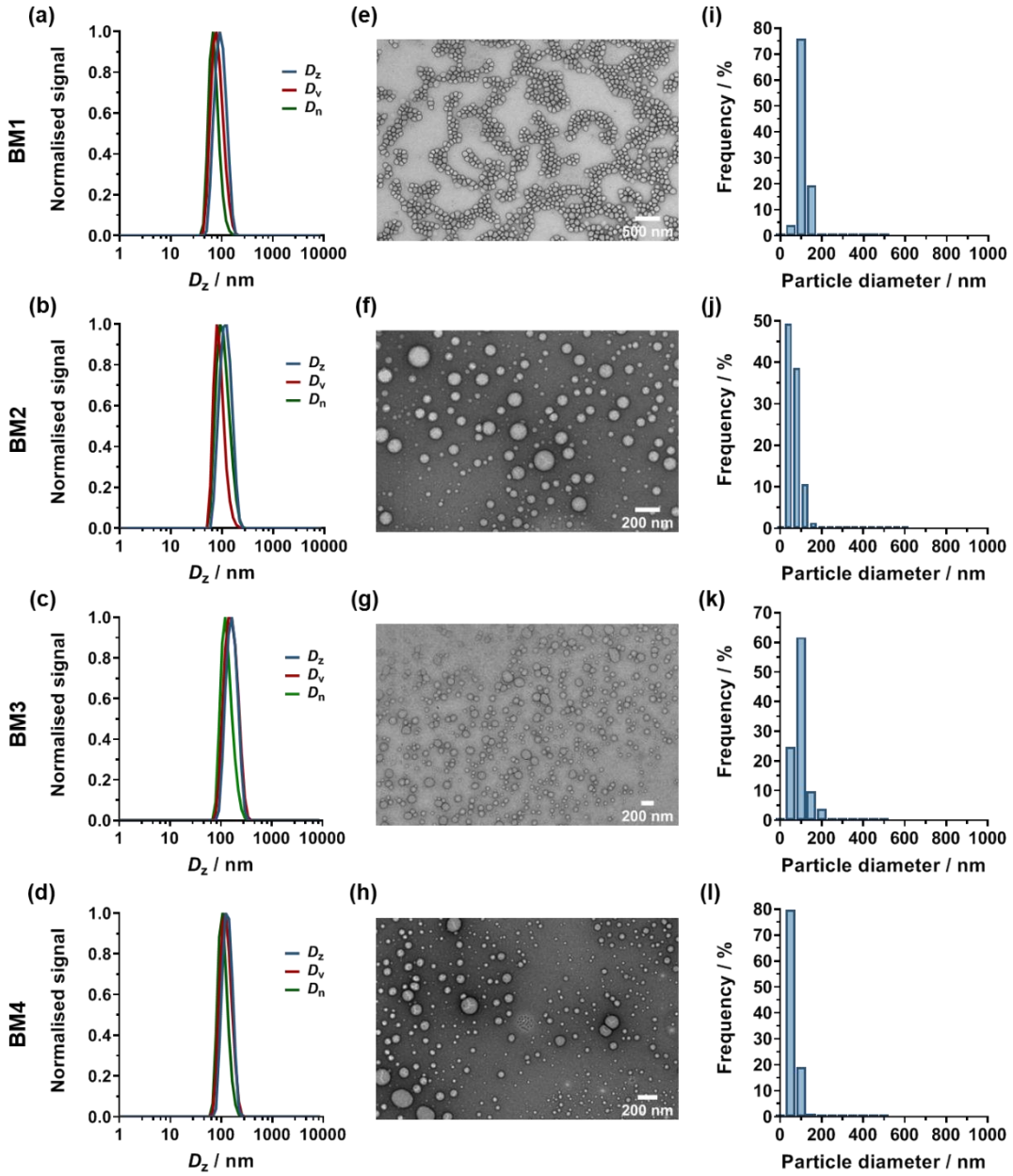

Figure 6. Colloidal characteristics of **OEG$_{23}$-L$_{150}$B** nanoparticles **BM1–BM4** after a 1:20 dilution in DMF and dialysis against water: (a–d) average diameters from DLS reported in number (D_n), volume (D_v) and intensity (D_z) distribution after formulation; (e–h) representative TEM images and (i–l) particle size distributions (n = 150–1200). TEM data (D_n, D_w, D_z, and PDI) are in Table S8.

3.2.3 Application to MDO. Even if rROPISA in heptane with MDO as a CKA was successful, it gave high dispersities up to 4 and thus a partial loss of control.[38] Herein, rROPISA in DMF under similar conditions achieved a much better control of the

copolymerization (Table S9) with M_n = 14.1–19.2 kg.mol^{-1} and $Đ$ = 1.57–1.80. ^{1}H NMR spectroscopy attested that **OEG$_{23}$-L$_{150}$M** copolymers were synthesized (Figure S9a) with F_{MDO} = 0.08–0.15, depending on the initial comonomer feed.

All copolymers exhibited nearly complete degradation under accelerated conditions (Figure S9b) and excellent agreement with the predicted values (Table S10, Figure S7e–h), suggesting a very high proportion of open MDO. The same transfer procedure to water resulted in stable nanoparticles with spherical morphologies and narrow PSD as observed by DLS and TEM, except for $f_{MDO,0}$ = 0.7 (**M4**) that also gave a fraction of microparticles (Figure 7). Not only was there no significant variation in their average diameters after dialysis against water (D_z = 131–170 nm), but they were also fairly constant regardless of copolymer composition (Figure S3, S8b, Table S9).

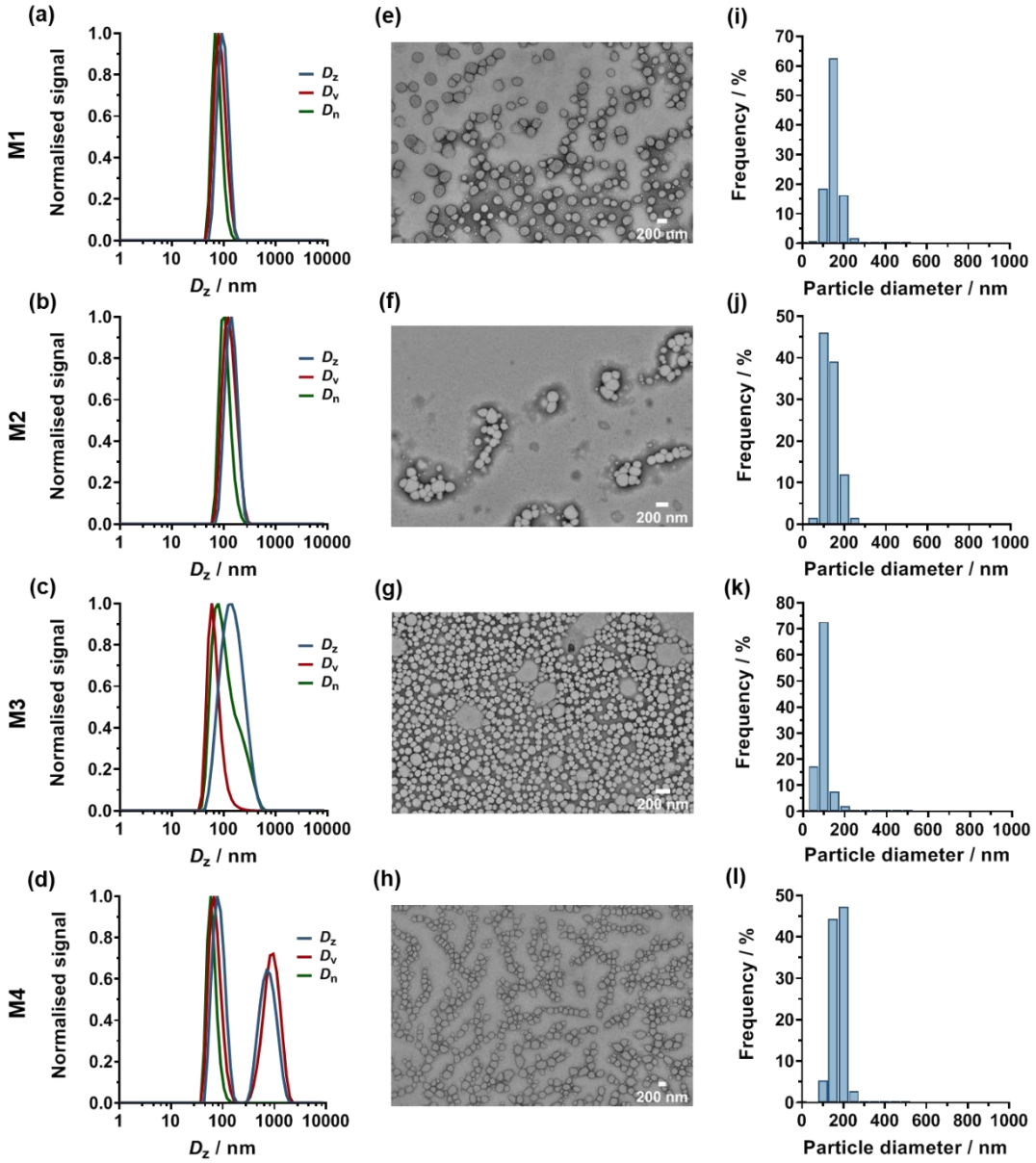

Figure 7. Colloidal characteristics of **OEG$_{23}$-L$_{150}$M** nanoparticles **M1**–**M4** after a 1:20 dilution in DMF and dialysis against water: (a–d) average diameters from DLS reported in number (D_n), volume (D_v) and intensity (D_z) distribution after formulation; (e–h) Representative TEM images and (i–l) particle size distributions (n = 200–500). TEM data (D_n, D_w, D_z, and PDI) are in Table S11.

Importantly, **OEG$_{23}$-L$_{150}$M** nanoparticles in DMF could also be directly dialysed against water, thus maintaining their original concentrations as opposed to **OEG$_{23}$-L$_{150}$MP** and **OEG$_{23}$-L$_{150}$B** nanoparticles that required a preliminary 1:20

dilution in DMF (Figure S10 and S11). **OEG$_{23}$-L$_{150}$M** nanoparticles exhibited colloidal stability as high as the other nanoparticles, well-preserved average diameters and narrow PSD (D_z = 113–154 nm, PSD = 0.03–0.14) up to F_{MDO} = 0.13 (Table S12).

3.3 Optimization of the transfer to water

The rROPISA process was then further optimized to allow all types of CKA-containing nanoparticles to be obtained in water without preliminary dilution, thus maximizing their aqueous concentrations. As previously hypothesized, we suspected that, for high $f_{CKA,0}$ values, unreacted MPDL/BMDO caused colloidal instability of **OEG$_{23}$-L$_{150}$MP** and **OEG$_{23}$-L$_{150}$B** nanoparticles during their dialysis against water. This limitation was resolved by performing an intermediate dialysis against acetone. Not only the unreacted monomer was efficiently removed, as shown by ^{1}H-NMR (Figure S12), but it also enabled the resultant nanoparticles to be successfully transferred to water by dialysis without dilution, even for the highest $f_{CKA,0}$ values (Figure S13). DLS measurements mostly showed little variation in diameters when passing from acetone to water and confirmed the excellent colloidal characteristics of **OEG$_{23}$-L$_{150}$MP** and **OEG$_{23}$-L$_{150}$B** nanoparticles in water in terms of size and particle size distribution (Figure 8 and Table S13). Average diameter in acetone was ~140 nm (PSD ~0.08) while in water it reached ~120 nm (PSD ~0.11). This procedure was also successfully applied to **OEG$_{52}$-L$_{300}$MP** and **OEG$_{23}$-L$_{150}$M** nanoparticles to show the versatility of the process. These two additional series of

nanoparticles exhibited great colloidal stability with good preservation of their average diameters, despite slight broadening of the PSD for the highest CKA contents (Table S13).

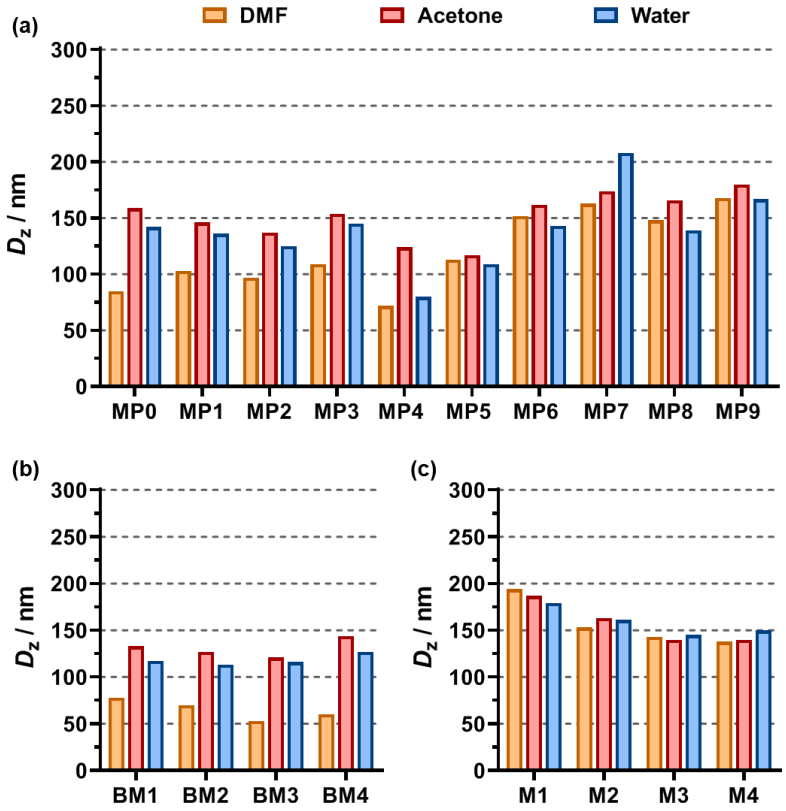

Figure 8. Intensity-average diameters of: (a) **OEG_{23}-L_{150}MP** (**MP0-MP4**) and **OEG_{52}-L_{300}MP** (**MP5-MP9**); (b) **OEG_{23}-L_{150}B** (**BM1-BM4**) and (c) **OEG_{23}-L_{150}M** (**M1-M4**) nanoparticles in DMF (orange bars), after direct dialysis against acetone (red bars) and followed by dialysis against water (blue bars).

Interestingly, cryo-TEM was used as a complementary technique to TEM and confirmed the spherical morphology for **OEG_{23}-L_{150}MP** and **OEG_{52}-L_{300}MP** nanoparticles (Figure S14), in good agreement with DLS data (Table S13) and TEM observations of their counterparts obtained without intermediate dialysis in acetone (Table S2).

3.4 Comparison with the nanoprecipitation technique

Compared to the traditional nanoprecipitation of preformed polymers, this two-step rROPISA process has the following advantages: (i) it allows the synthesis of nanoparticles without any surfactant, thus avoiding the purification of the nanoparticles to remove free/weakly adsorbed surfactant; (ii) much higher solids content nanoparticles can be obtained (e.g., **MP5–8** nanoparticles exhibit final concentrations ranging from 16 up to 75 $mg.mL^{-1}$ (measured by gravimetry) compared to typically ~5–10 $mg.mL^{-1}$ for polymer nanoparticles obtained by nanoprecipitation) and (iii) it produces better-defined nanoparticles with lower average diameters and particle size distributions.

To illustrate this last point, we performed the nanoprecipitation of purified copolymers **MP7** (Table S2) with targeted concentrations ranging from 2 to 20 $mg.mL^{-1}$ (note that colloidal instability in the long run was observed at 20 $mg.mL^{-1}$) in order to establish a point-by-point comparison with **MP7** nanoparticles directly obtained by the two-step rROPISA process (Table S14). **MP7** nanoparticles obtained by rROPISA after diluted dialysis (2 $mg.mL^{-1}$) exhibited the lowest average diameters (D_z = 155 nm) and PSD (0.08), whereas the nanoprecipitation of **MP7** at 2 $mg.mL^{-1}$ produced nanoparticles of ~200 nm in diameter (Figure S15). Increasing the nanoparticle concentration during nanoprecipitation further increased the average diameters that reached 267 nm at 20 $mg.mL^{-1}$ and gave a broad PSD (0.26). Also, **MP7** nanoparticles obtained after intermediate dialysis (34 $mg.mL^{-1}$) exhibited

superior colloidal characteristics than those obtained by nanoprecipitations above 2 $mg.mL^{-1}$.

3.5 Degradation of the nanoparticles

After having shown the tunable hydrolytic degradation of the copolymers under accelerated conditions, degradation of the nanoparticles in aqueous suspension was investigated in 2.5 wt.% KOH at 37 °C. Nanoparticles responded quickly to hydrolysis (< 24 h) and exhibited tunable degradation as function of F_{CKA} with decrease in M_n up to > 95% (Figure S16 and 9). Overall, the degradation kinetics and the final M_ns after degradation of the different copolymer nanoparticles were similar to those of the corresponding free copolymers.

These results suggested that, regardless of the CKA used, important water uptake by the nanoparticles successfully occurred, resulting in significant degradation. It is also worth noting that this is the first time that extensive hydrolytic degradation of CKA-containing nanoparticles synthesized by polymerization in dispersed medium is reported.

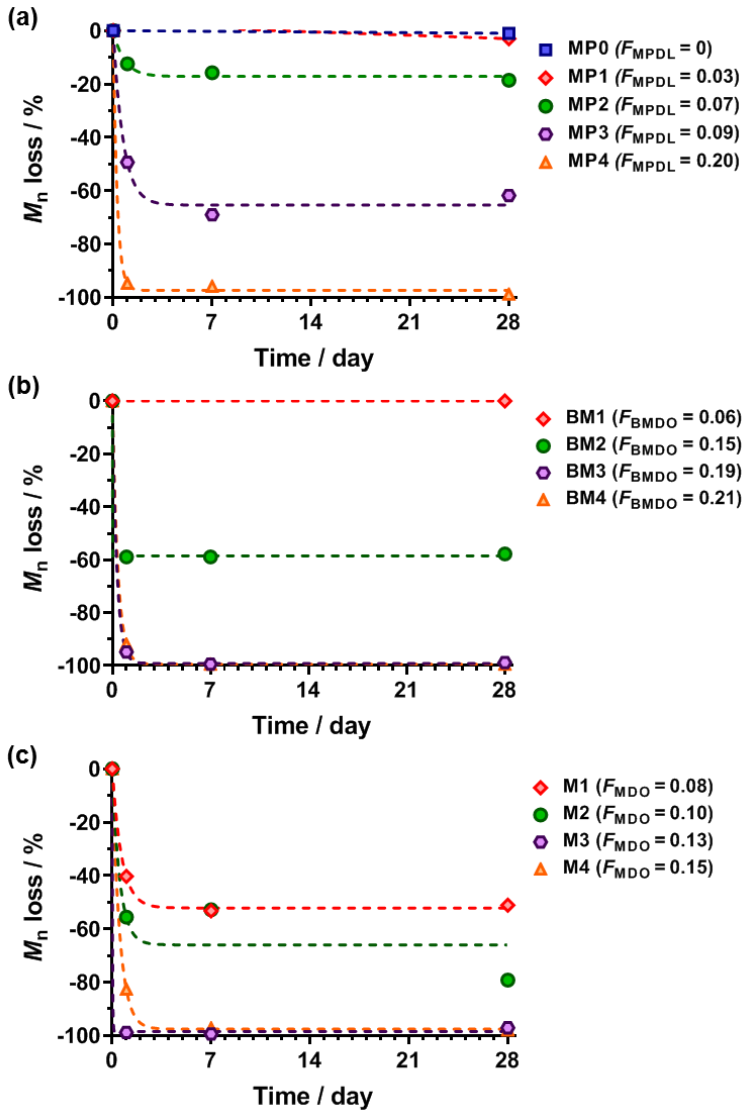

Figure 9. Evolution with time of the number-average molar mass (M_n) loss during degradation under accelerated conditions (2.5% KOH in water) of **OEG$_{23}$-L$_{150}$CKA** copolymer nanoparticles with the molar fraction of CKA (F_{CKA}) in the copolymer: (a) **OEG$_{23}$-L$_{150}$MP** (**MP0-MP4**) copolymers nanoparticles (F_{MPDL} = 0–0.20); (b) **OEG$_{23}$-L$_{150}$BM** (**BM1-BM4**) copolymers nanoparticles (F_{BMDO}= 0.06–0.21) and (c) **OEG$_{23}$-L$_{150}$M** (**M1-M4**) copolymers nanoparticles (F_{MDO} = 0.08–0.15). Dashed lines represent the exponential one phase decay fit. Since SEC is known to overestimate the molar masses at the low-molar-mass region, these values should be taken with care.

3.6 Cytocompatibility

To show the broad applicability of these degradable vinyl copolymer nanoparticles, and for instance to consider their use for biomedical applications, their

cytocompatibility was tested on three representative healthy cell lines via both cell viability assays and cell morphology observations. The cell lines used were: (i) murine macrophages (J774.A1), which are monocyte cells that play a key role in phagocytosis; (ii) human umbilical vein endothelial cells (HUVEC), which are widely used primary endothelial cells for in vitro studies of the vasculature and (iii) murine fibroblasts (NIH/3T3), which are one of the most commonly used fibroblast cell lines. Although there have been examples of cytocompatible CKA-containing copolymers and copolymers formulated into nanoparticles,[9,45,52,53] the cytocompatibility of CKA-containing nanoparticles obtained by polymerization in dispersed media towards healthy cells has never been investigated.

Three representative libraries of nanoparticles were selected: (i) **OEG_{23}-L_{150}MP** and **OEG_{23}-L_{150}M**, to investigate potential influence of the nature of the CKA and (ii) **OEG_{52}-L_{300}MP**, to evaluate the effect of the POEGMA block length. For each series of nanoparticles, the CKA content was varied ($f_{CKA,0}$ = 0–0.7) to probe its effect on the cell viability. Note that **OEG_{23}-L_{150}B** nanoparticles were not tested due to their structural similarity to **OEG_{23}-L_{150}MP** nanoparticles. Overall, all types of nanoparticles exhibited cell viability in the 70–100% range up to 0.1 mg.mL^{-1} for NIH/3T3 cells and up to 0.5 mg.mL^{-1} for J774.A1 and HUVEC cells (Figure 10a-c). It should be noted that these relatively high concentrations do not reflect their expected use but would rather overexpress any cytotoxic effects arising from the copolymer structures or from their degradation products. Interestingly, despite their sensitivity to foreign materials due to their phagocytic functions resulting in engulfment of

nanoparticles, macrophages (J774.A1 cells) exhibited cell viability greater than 80% for all nanoparticle concentrations.

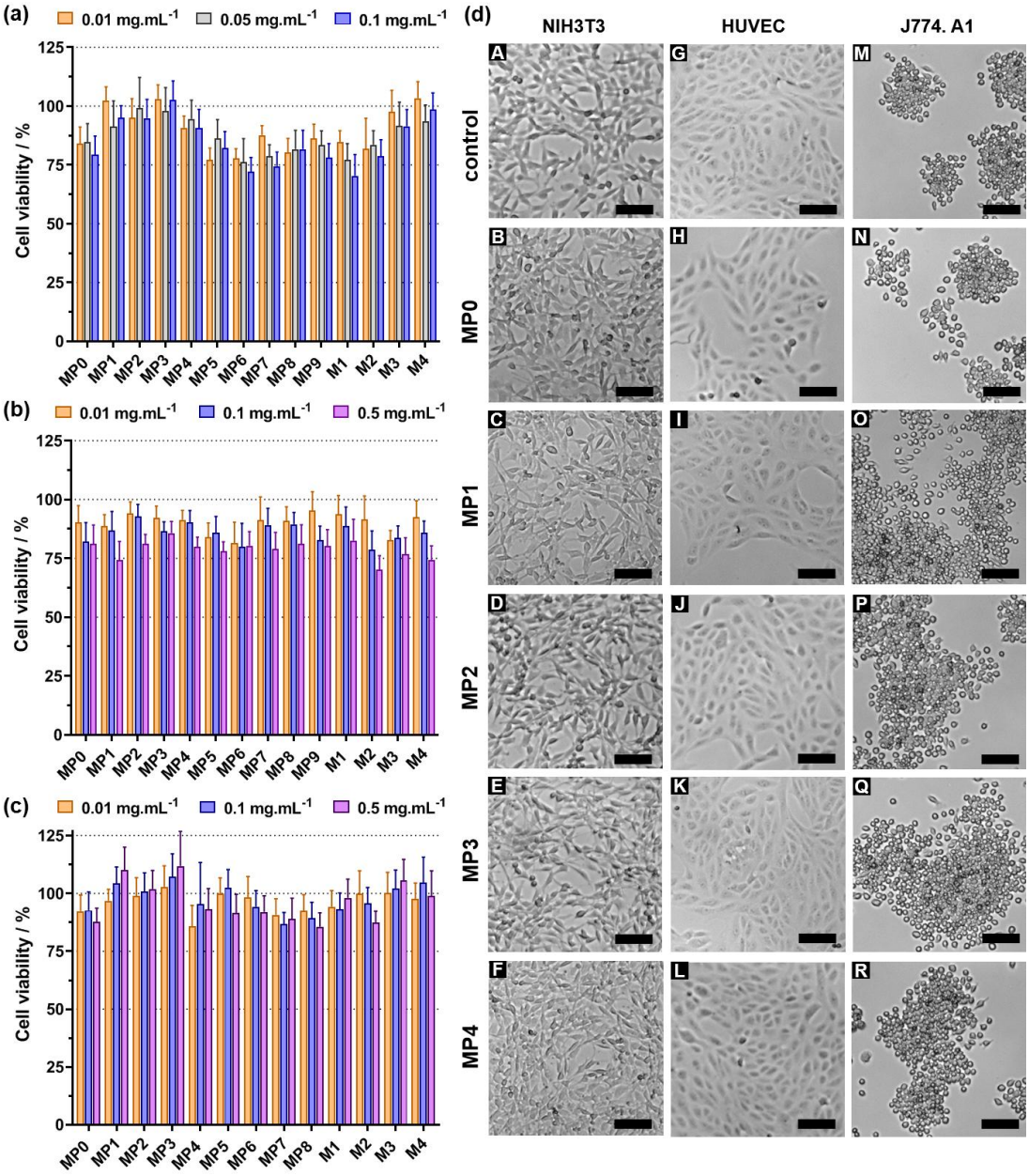

Figure 10. Cell viability (MTT assay) after incubation of: (a) NIH/3T3 cells; (b) HUVEC cells and (c) J774.A1 cells with **OEG$_m$-L$_n$MP** ($f_{MPDL,0}$ = 0–0.7, **MP0-MP9**) and **OEG$_{23}$-L$_{150}$M** ($f_{MDO,0}$ = 0.2–0.7, **M1-M4**) nanoparticles at different concentrations. Results were expressed as percentage of absorption of treated cells ± SD in comparison with untreated cells (control). (d) Representative optical images of NIH/3T3 (A-F), HUVEC

(G-L), and J774.A1 cells (M-R) after incubation for 72 h with **MP0**-**MP4** nanoparticles at 0.1 $mg.mL^{-1}$. Scale bar = 100 µm.

Looking at each set of results individually, it appeared that increasing the nanoparticle concentration over this range had no significant influence on the viability of J774.A1 and NIH/3T3 cells, and only little influence on that of HUVEC cells (especially for **OEG_{23}-L_{150}M** nanoparticles), which seems to corroborate previous cytocompatibility studies on CKA-containing water-soluble copolymers.[52] Increasing the amount of CKA however seemed to conduct to higher cell viabilities of NIH/3T3 cells especially for **OEG_{23}-L_{150}MP** and **OEG_{23}-L_{150}M** nanoparticles. No significant effect was observed on the three cell lines when increasing the POEGMA chain length with **OEG_{52}-L_{300}MP** nanoparticles.

An observation of cell morphology was performed after a 72-hour incubation period of the three cell lines with the nanoparticles at the same concentrations as a complementary method to the cell viability assays to assess their cytocompatibility (Figure 10d and Figure S17-24). Overall, cells treated with the nanoparticles, whatever their nature, exhibited no noticeable difference in terms of morphology (e.g., round-like shape for J774.A1 cells, cobblestone-like morphology for HUVEC cells and fibroblast-like shape for NIH/3T3 cells), size, density or cell proliferation compared to untreated cells, thus confirming the results from the cell viability assays. Therefore, there was no adverse effect of nanoparticles at these concentrations, regardless of the nature of the CKAs tested, their content and the two different POEGMA chain lengths. In conclusion, all these results attested for their cytocompatibility and are promising for their ultimate biocompatibility.

4. Conclusion

In this study, we reported on a simple two-step rROPISA process that allowed to readily produce stable, aqueous suspensions of mostly narrowly dispersed, degradable vinyl copolymer nanoparticles. It relied on RAFT-mediated copolymerization of LMA and CKA in DMF at 15 wt.% solid contents from a solvophilic POEGMA macro-CTA. The resulting nanoparticles were then transferred to water by simple dialysis during which their colloidal properties were maintained.

Several key structural parameters were varied such as the nature of the CKA, its content in the copolymer and the POEGMA macro-CTA chain length. It was shown that this two-step rROPISA process was perfectly applicable to the three main CKAs use in rROP (i.e., MPDL, BMDO and MDO) and led to tunable CKA contents up to 21 mol.%, thus demonstrating its versatility and robustness. Increasing the POEGMA chain length helped to improve the colloidal properties upon transfer to water especially for high CKA contents. While MDO-containing nanoparticles could be directly transferred to water, the two-step rROPISA process was further optimized for MPDL- and BMDO-containing copolymers by adding an intermediate dialysis in acetone. It allowed both high concentrations of narrowly dispersed nanoparticles in water to be obtained in the 80–250 nm range and removal of unreacted monomer.

Degradation experiments showed that both free copolymers and corresponding nanoparticles were degradable under accelerated conditions depending on their CKA

content. Cytotoxicity studies performed on several libraries of nanoparticles via cell viability assays and cell morphology observations, showed no cytotoxicity up to 0.1 or 0.5 $mg.mL^{-1}$ on three representative healthy cell lines. With their PEG-based shell, which is known to confer stealth properties, these results make it possible to envisage the use of these nanoparticles in the biomedical field.

Given its benefits, we believe such a polymerization process to be a promising tool to generate degradable vinyl polymer nanoparticles with great potential for drug delivery applications. Importantly, such approach could also be beneficial to other research fields as degradable particles could favorably replace traditional latexes to yield more environmentally friendly materials. In this context, this two-step rROPISA process could be an important step forward against plastic pollution which has become one of the most pressing environmental problems.

Supporting Information

Supporting Information Available. Macromolecular characteristics (^{1}H NMR, SEC) of POEGMA macro-CTAs, macromolecular (^{1}H NMR, SEC) and colloidal (DLS, TEM) characteristics of copolymer nanoparticles **MP0–9**, **BM1–4** and **M1–4**, before and after dialysis (direct, diluted or with intermediate dialysis against acetone), and before and during degradation, pictures of nanoparticle samples **MP0–9**, **BM1–4** and **M1–4**, cryo-TEM images of copolymer nanoparticles **MP0–9** after dialysis against acetone and against water, colloidal characteristics (DLS) of **MP7** nanoparticles obtained by nanoprecipitation, SEC chromatograms of copolymers **MP0–4**, **BM1–4** and **M1–4** during degradation, optical images of HUVEC, NIH/3T3 and J774.A1 cells after incubation with copolymer nanoparticles **MP0–9** and **M1–4**. This information is available free of charge via the Internet at http://pubs.acs.org/.

Acknowledgement

We thank the China Scholarship Council (CSC) for the PhD fellowship (2017-2021) of CZ. The authors thank Claire Boulogne and Cynthia Gillet (I2BC, Gif-sur-Yvette, France) for technical assistance in TEM, Ana-Andreea Arteni and Malika Ouldali (I2BC, UMR 9198 Institut de Biologie Intégrative de la Cellule, Gif-sur-Yvette, France) for technical assistance in Cyro-TEM and Valerie Nicolas (MIPSIT, Châtenay-Malabry, France) for the technical assistance in optical microscopy. The CNRS is also acknowledged for financial support.

Table of Content

A simple two-step radical ring-opening copolymerization-induced self-assembly (rROPISA) process allows to readily produce stable, aqueous suspensions of narrowly dispersed, degradable vinyl copolymer nanoparticles comprising ester groups in the copolymer backbone.

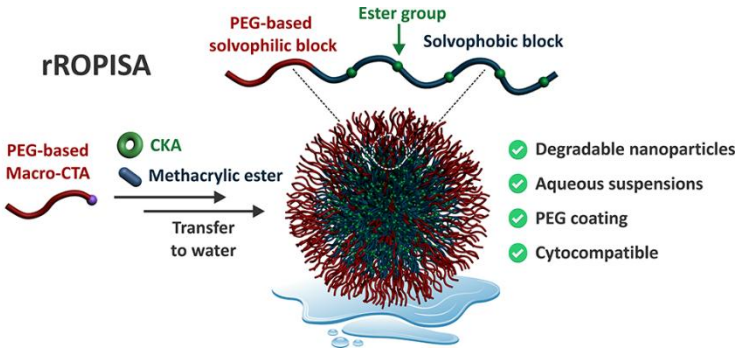

5. Reference

1. Safra, T.; Muggia, F.; Jeffers, S.; Tsao-Wei, D. D.; Groshen, S.; Lyass, O.; Henderson, R.; Berry, G.; Gabizon, A. Pegylated Liposomal Doxorubicin (Doxil): Reduced Clinical Cardiotoxicity in Patients Reaching or Exceeding Cumulative Doses of 500 Mg/M2. *Ann. Oncol.* **2000**, *11* (8), 1029–1034.

2. Couvreur, P.; Vauthier, C. Nanotechnology: Intelligent Design to Treat Complex Disease. *Pharm. Res.* **2006**, *23* (7), 1417–1450.
3. Soppimath, K. S.; Aminabhavi, T. M.; Kulkarni, A. R.; Rudzinski, W. E. Biodegradable Polymeric Nanoparticles as Drug Delivery Devices. *J. Controlled Release* **2001**, *70* (1–2), 1–20.
4. Liechty, W. B.; Kryscio, D. R.; Slaughter, B. V.; Peppas, N. A. Polymers for Drug Delivery Systems. *Annu. Rev. Chem. Biomol. Eng.* **2010**, *1*, 149–173.
5. Delplace, V.; Nicolas, J. Degradable Vinyl Polymers for Biomedical Applications. *Nat. Chem.* **2015**, *7* (10), 771–784.
6. Tardy, A.; Nicolas, J.; Gigmes, D.; Lefay, C.; Guillaneuf, Y. Radical Ring-Opening Polymerization: Scope, Limitations, and Application to (Bio)Degradable Materials. *Chem. Rev.* **2017**, *117* (3), 1319–1406.
7. Pesenti, T.; Nicolas, J. 100th Anniversary of Macromolecular Science Viewpoint: Degradable Polymers from Radical Ring-Opening Polymerization: Latest Advances, New Directions, and Ongoing Challenges. *ACS Macro Lett.* **2020**, *9* (12), 1812–1835.
8. Delplace, V.; Harrisson, S.; Tardy, A.; Gigmes, D.; Guillaneuf, Y.; Nicolas, J. Nitroxide-Mediated Radical Ring-Opening Copolymerization: Chain-End Investigation and Block Copolymer Synthesis. *Macromol. Rapid Commun.* **2014**, *35* (4), 484–491.
9. Siebert, J. M.; Baumann, D.; Zeller, A.; Mailänder, V.; Landfester, K. Synthesis of Polyester Nanoparticles in Miniemulsion Obtained by Radical Ring-Opening of BMDO and Their Potential as Biodegradable Drug Carriers. *Macromol. Biosci.* **2012**, *12* (2), 165–175.
10. Penfold, N. J. W.; Yeow, J.; Boyer, C.; Armes, S. P. Emerging Trends in Polymerization-Induced Self-Assembly. *ACS Macro Lett.* **2019**, *8* (8), 1029–1054.
11. Warren, N. J.; Armes, S. P. Polymerization-Induced Self-Assembly of Block Copolymer Nano-Objects via RAFT Aqueous Dispersion Polymerization. *J. Am. Chem. Soc.* **2014**, *136* (29), 10174–10185.
12. Canning, S. L.; Smith, G. N.; Armes, S. P. A Critical Appraisal of RAFT-Mediated Polymerization-Induced Self-Assembly. *Macromolecules* **2016**, *49* (6), 1985–2001.
13. Gurnani, P.; Bray, C. P.; Richardson, R. A. E.; Peltier, R.; Perrier, S. Heparin-Mimicking Sulfonated Polymer Nanoparticles via RAFT Polymerization-Induced Self-Assembly. *Macromol. Rapid Commun.* **2019**, *40* (2), 1800314.
14. Zhang, W.-J.; Hong, C.-Y.; Pan, C.-Y. Fabrication of Spaced Concentric Vesicles and Polymerizations in RAFT Dispersion Polymerization. *Macromolecules* **2014**, *47* (5), 1664–1671.
15. Warren, N. J.; Mykhaylyk, O. O.; Ryan, A. J.; Williams, M.; Doussineau, T.; Dugourd, P.; Antoine, R.; Portale, G.; Armes, S. P. Testing the Vesicular Morphology to Destruction: Birth and Death of Diblock Copolymer Vesicles Prepared via Polymerization-Induced Self-Assembly. *J. Am. Chem. Soc.* **2015**, *137* (5), 1929–1937.
16. Gonzato, C.; Semsarilar, M.; Jones, E. R.; Li, F.; Krooshof, G. J. P.; Wyman, P.; Mykhaylyk, O. O.; Tuinier, R.; Armes, S. P. Rational Synthesis of Low-Polydispersity Block Copolymer Vesicles in Concentrated Solution via Polymerization-Induced Self-Assembly. *J. Am. Chem. Soc.* **2014**, *136* (31), 11100–11106.

17. Penfold, N. J. W.; Whatley, J. R.; Armes, S. P. Thermoreversible Block Copolymer Worm Gels Using Binary Mixtures of PEG Stabilizer Blocks. *Macromolecules* **2019**, *52* (4), 1653–1662.
18. Wright, D. B.; Touve, M. A.; Adamiak, L.; Gianneschi, N. C. ROMPISA: Ring-Opening Metathesis Polymerization-Induced Self-Assembly. *ACS Macro Lett.* **2017**, *6* (9), 925–929.
19. Wang, G.; Schmitt, M.; Wang, Z.; Lee, B.; Pan, X.; Fu, L.; Yan, J.; Li, S.; Xie, G.; Bockstaller, M. R.; Matyjaszewski, K. Polymerization-Induced Self-Assembly (PISA) Using ICAR ATRP at Low Catalyst Concentration. *Macromolecules* **2016**, *49* (22), 8605–8615.
20. Sha, Y.; Rahman, M. A.; Zhu, T.; Cha, Y.; McAlister, C. W.; Tang, C. ROMPI-CDSA: Ring-Opening Metathesis Polymerization-Induced Crystallization-Driven Self-Assembly of Metallo-Block Copolymers. *Chem. Sci.* **2019**, *10* (42), 9782–9787.
21. Varlas, S.; Foster, J. C.; Georgiou, P. G.; Keogh, R.; Husband, J. T.; Williams, D. S.; O'Reilly, R. K. Tuning the Membrane Permeability of Polymersome Nanoreactors Developed by Aqueous Emulsion Polymerization-Induced Self-Assembly. *Nanoscale* **2019**, *11* (26), 12643–12654.
22. Wang, X.; Man, S.; Zheng, J.; An, Z. Alkyl α-Hydroxymethyl Acrylate Monomers for Aqueous Dispersion Polymerization-Induced Self-Assembly. *ACS Macro Lett.* **2018**, *7* (12), 1461–1467.
23. Yeow, J.; Sugita, O. R.; Boyer, C. Visible Light-Mediated Polymerization-Induced Self-Assembly in the Absence of External Catalyst or Initiator. *ACS Macro Lett.* **2016**, *5* (5), 558–564.
24. Le, D.; Wagner, F.; Takamiya, M.; Hsiao, I.-L.; Gil Alvaradejo, G.; Strähle, U.; Weiss, C.; Delaittre, G. Straightforward Access to Biocompatible Poly(2-Oxazoline)-Coated Nanomaterials by Polymerization-Induced Self-Assembly. *Chem. Commun.* **2019**, *55* (26), 3741–3744.
25. Ding, Y.; Zhao, Q.; Wang, L.; Huang, L.; Liu, Q.; Lu, X.; Cai, Y. Polymerization-Induced Self-Assembly Promoted by Liquid–Liquid Phase Separation. *ACS Macro Lett.* **2019**, *8* (8), 943–946.
26. Dong, S.; Zhao, W.; Lucien, F. P.; Perrier, S.; Zetterlund, P. B. Polymerization Induced Self-Assembly: Tuning of Nano-Object Morphology by Use of CO2. *Polym. Chem.* **2015**, *6* (12), 2249–2254.
27. Figg, C. A.; Simula, A.; Gebre, K. A.; Tucker, B. S.; Haddleton, D. M.; Sumerlin, B. S. Polymerization-Induced Thermal Self-Assembly (PITSA). *Chem. Sci.* **2015**, *6* (2), 1230–1236.
28. Yeow, J.; Xu, J.; Boyer, C. Polymerization-Induced Self-Assembly Using Visible Light Mediated Photoinduced Electron Transfer–Reversible Addition–Fragmentation Chain Transfer Polymerization. *ACS Macro Lett.* **2015**, *4* (9), 984–990.
29. Karagoz, B.; Esser, L.; Duong, H. T.; Basuki, J. S.; Boyer, C.; Davis, T. P. Polymerization-Induced Self-Assembly (PISA) – Control over the Morphology of Nanoparticles for Drug Delivery Applications. *Polym. Chem.* **2014**, *5* (2), 350–355.
30. Zhao, W.; Ta, H. T.; Zhang, C.; Whittaker, A. K. Polymerization-Induced Self-Assembly (PISA) - Control over the Morphology of 19F-Containing Polymeric

Nano-Objects for Cell Uptake and Tracking. *Biomacromolecules* **2017**, *18* (4), 1145–1156.

31. Zhang, W.-J.; Hong, C.-Y.; Pan, C.-Y. Fabrication of Reductive-Responsive Prodrug Nanoparticles with Superior Structural Stability by Polymerization-Induced Self-Assembly and Functional Nanoscopic Platform for Drug Delivery. *Biomacromolecules* **2016**, *17* (9), 2992–2999.
32. Zhang, W.-J.; Hong, C.-Y.; Pan, C.-Y. Polymerization-Induced Self-Assembly of Functionalized Block Copolymer Nanoparticles and Their Application in Drug Delivery. *Macromol. Rapid Commun.* **2019**, *40* (2), 1800279.
33. Blackman, L. D.; Varlas, S.; Arno, M. C.; Fayter, A.; Gibson, M. I.; O'Reilly, R. K. Permeable Protein-Loaded Polymersome Cascade Nanoreactors by Polymerization-Induced Self-Assembly. *ACS Macro Lett.* **2017**, *6* (11), 1263–1267.
34. Kaga, S.; Truong, N. P.; Esser, L.; Senyschyn, D.; Sanyal, A.; Sanyal, R.; Quinn, J. F.; Davis, T. P.; Kaminskas, L. M.; Whittaker, M. R. Influence of Size and Shape on the Biodistribution of Nanoparticles Prepared by Polymerization-Induced Self-Assembly. *Biomacromolecules* **2017**, *18* (12), 3963–3970.
35. Ladmiral, V.; Semsarilar, M.; Canton, I.; Armes, S. P. Polymerization-Induced Self-Assembly of Galactose-Functionalized Biocompatible Diblock Copolymers for Intracellular Delivery. *J. Am. Chem. Soc.* **2013**, *135* (36), 13574–13581.
36. Grazon, C.; Salas-Ambrosio, P.; Ibarboure, E.; Buol, A.; Garanger, E.; Grinstaff, M. W.; Lecommandoux, S.; Bonduelle, C. Aqueous Ring-Opening Polymerization-Induced Self-Assembly (ROPISA) of N-Carboxyanhydrides. *Angew. Chem. Int. Ed.* **2020**, *59* (2), 622–626.
37. Guegain, E.; Zhu, C.; Giovanardi, E.; Nicolas, J. Radical Ring-Opening Copolymerization-Induced Self-Assembly (RROPISA). *Macromolecules* **2019**, *52* (10), 3612–3624.
38. Zhu, C.; Nicolas, J. Towards Nanoparticles with Site-Specific Degradability by Ring-Opening Copolymerization Induced Self-Assembly in Organic Medium. *Polym. Chem.* **2021**, *12* (4), 594–607.
39. Veronese, F. M. Peptide and Protein PEGylation: A Review of Problems and Solutions. *Biomaterials* **2001**, *22* (5), 405–417.
40. F. Veronese and J.M. Harris. Introduction and Overview of Peptide and Protein Pegylation. *Adv. Drug Deliv. Rev.* **2002**, *54* (4), 453–456.
41. Roberts, M. J.; Bentley, M. D.; Harris, J. M. Chemistry for Peptide and Protein PEGylation. *Adv. Drug Deliv. Rev.* **2002**, *54* (4), 459–476.
42. Duncan, R. The Dawning Era of Polymer Therapeutics. *Nat. Rev. Drug Discov.* **2003**, *2* (5), 347–360.
43. Harris, J. M.; Chess, R. B. Effect of Pegylation on Pharmaceuticals. *Nat. Rev. Drug Discov.* **2003**, *2* (3), 214–221.
44. Tran, J.; Guégain, E.; Ibrahim, N.; Harrisson, S.; Nicolas, J. Efficient Synthesis of 2-Methylene-4-Phenyl-1,3-Dioxolane, a Cyclic Ketene Acetal for Controlling the NMP of Methyl Methacrylate and Conferring Tunable Degradability. *Polym. Chem.* **2016**, *7* (26), 4427–4435.

45. Guégain, E.; Tran, J.; Deguettes, Q.; Nicolas, J. Degradable Polymer Prodrugs with Adjustable Activity from Drug-Initiated Radical Ring-Opening Copolymerization. *Chem. Sci.* **2018**, *9* (43), 8291–8306.
46. Stolnik, S.; Illum, L.; Davis, S. S. Long Circulating Microparticulate Drug Carriers. *Adv. Drug Deliv. Rev.* **1995**, *16* (2–3), 195–214.
47. Gref, R.; Minamitake, Y.; Peracchia, M.; Trubetskoy, V.; Torchilin, V.; Langer, R. Biodegradable Long-Circulating Polymeric Nanospheres. *Science* **1994**, *263* (5153), 1600–1603.
48. Storm, G.; Belliot, S. O.; Daemen, T.; Lasic, D. D. Surface Modification of Nanoparticles to Oppose Uptake by the Mononuclear Phagocyte System. *Adv. Drug Deliv. Rev.* **1995**, *17* (1), 31–48.
49. Malikmammadov, E.; Tanir, T. E.; Kiziltay, A.; Hasirci, V.; Hasirci, N. PCL and PCL-Based Materials in Biomedical Applications. *J. Biomater. Sci. Polym. Ed.* **2018**, *29* (7–9), 863–893.
50. Hill, M. R.; Guégain, E.; Tran, J.; Figg, C. A.; Turner, A. C.; Nicolas, J.; Sumerlin, B. S. Radical Ring-Opening Copolymerization of Cyclic Ketene Acetals and Maleimides Affords Homogeneous Incorporation of Degradable Units. *ACS Macro Lett.* **2017**, *6* (10), 1071–1077.
51. Dalgakiran, E.; Tatlipinar, H. The Role of Hydrophobic Hydration in the LCST Behaviour of POEGMA300 by All-Atom Molecular Dynamics Simulations. *Phys. Chem. Chem. Phys.* **2018**, *20* (22), 15389–15399.
52. Delplace, V.; Tardy, A.; Harrisson, S.; Mura, S.; Gigmes, D.; Guillaneuf, Y.; Nicolas, J. Degradable and Comb-Like PEG-Based Copolymers by Nitroxide-Mediated Radical Ring-Opening Polymerization. *Biomacromolecules* **2013**, *14* (10), 3769–3779.
53. Tran, J.; Pesenti, T.; Cressonnier, J.; Lefay, C.; Gigmes, D.; Guillaneuf, Y.; Nicolas, J. Degradable Copolymer Nanoparticles from Radical Ring-Opening Copolymerization between Cyclic Ketene Acetals and Vinyl Ethers. *Biomacromolecules* **2019**, *20* (1), 305–317.